
Imaging Experimental Atherosclerotic Lesions in ApoE Knockout Mice: Enhanced Targeting with Z₂D₃-Anti-DTPA Bispecific Antibody and ^{99m}Tc-Labeled Negatively Charged Polymers

Ban-An Khaw¹, Yared Tekabe^{1,2}, and Lynne L. Johnson²

¹Center for Cardiovascular Targeting, School of Pharmacy, Bouve College of Health Sciences, Northeastern University, Boston, Massachusetts; and ²Division of Cardiology, Department of Medicine, Columbia University Medical Center, New York, New York

In vivo molecular imaging may be improved if specific radioactivity at the target site could be increased while maintaining low background activity. Bispecific antibody complexes and ^{99m}Tc-labeled negatively charged chelating polymers that react specifically with the capture arm of the bispecific antibody complex were used to demonstrate the feasibility of imaging very small atherosclerotic lesions in ApoE knockout mice. **Methods:** Left femoral artery denudation in ApoE^{-/-} mice on a hyperlipidemic diet was used to induce accelerated atherosclerotic lesions. Approximately 40 μg of bispecific antibodies were injected intravenously after 2 wk of endothelial denudation. The next day, ~15.0 MBq ^{99m}Tc-DTPA-succinyl-polylysine (2 μg; DTPA is diethylenetriaminepentaacetic acid) were injected intravenously. **Results:** In vivo γ-images showed that lesions were observed unequivocally by 2–3 h. Sham-operated right femoral regions showed no radiotracer accumulation. Ex vivo γ-scintillation counting corrected for sham-operated nonspecific activity and lesion mass showed that the mean lesion activity was 10.10 ± 6.76 %ID/g (percentage injected dose per gram), whereas nonspecific human IgG bispecific control (NSB control) also corrected similarly was 0.939 ± 0.877 %ID/g (*P* < 0.03). Atherosclerotic lesions were confirmed by immunohistochemical staining. Computer planimetry of immunohistograms showed the mean lesion size to be 2.64 ± 2.46 mg. **Conclusion:** Use of bispecific antibody complexes and ^{99m}Tc-DTPA-succinyl-polylysine enabled in vivo visualization of very small atherosclerotic lesions in ApoE knockout mice.

Key Words: bispecific antibody; pretargeting; radiolabeled polymer

J Nucl Med 2006; 47:868–876

Bispecific antibodies for diagnosis and therapy were first reported by Brennan et al. in 1985 (1). Subsequent to this seminal work, >700 peer-reviewed articles on pretargeted

bispecific antibody therapy have been published. In 1989, Le Doussal et al. reported pretargeting of cells in vitro and in vivo with bispecific antibodies and radiolabeled monovalent and divalent haptens (2,3). Direct radiolabeling of these haptens with radioisotopes such as ¹¹¹In, ^{99m}Tc, or ¹²³I for in vivo imaging has been reported. These radiotracers were developed to overcome limitations of high background antibody activity, especially in the liver, to visualize metastases in cancer imaging (4). Although pretargeted antibody imaging with mono- or divalent hapten technology provided images with lower background and less nontarget organ activities, we hypothesized that if the specific radioactivity at each antibody target site were increased, at the same time maintaining very low background activity, then very small lesions should be visualized by in vivo γ-imaging even with standard γ-cameras. Narula et al. demonstrated that experimental atherosclerotic lesions in rabbits can be visualized within 3 h if a very high specific radioactivity-labeled high antibody dose of Z₂D₃ F(ab')₂ were used in comparison with a lower specific radioactivity, low antibody dose (5). However, nontarget organ activity in these animals was still unacceptably high.

The approach we have taken to improve in vivo molecular imaging is to use a bispecific antibody. The targeting arm consists of chimeric Z₂D₃ F(ab')₂ antibody, which is specific for a lipid antigen complex produced by proliferating smooth muscle cells (SMCs) of atherosclerotic lesions or postangioplasty restenosis, and a murine anti-DTPA monoclonal F(ab')₂ antibody (6C31H3; DTPA is diethylenetriaminepentaacetic acid) as the capture arm. A negatively charged, high specific radioactivity ^{99m}Tc-DTPA-succinylated polylysine polymer (^{99m}Tc-DTPA-Suc-PL_{14.6} kDa) is used as the radiopharmaceutical that will be captured by the capture arm of the pretargeted bispecific antibody. This 2-step targeting approach not only reduced the nontarget background activities but also enabled enhanced unequivocal visualization of very small femoral artery atherosclerotic lesions in ApoE^{-/-} mice within 2–3 h after intravenous administration of the radiotracer.

Received Oct. 18, 2005; revision accepted Jan. 9, 2006.
For correspondence or reprints contact: Ban-An Khaw, PhD, Center for Cardiovascular Targeting, School of Pharmacy, Bouve College of Health Sciences, Northeastern University, Boston, MA 02115
E-mail: b.khaw@neu.edu

MATERIALS AND METHODS

Antibodies and Preparation of F(ab')₂

Chimeric Z₂D₃ and anti-DTPA 6C31H3 antibodies were prepared and purified as described (6). Purified Z₂D₃ or 6C31H3 antibodies were subjected to digestion with immobilized pepsin beads (Sigma Chemical Co.) (7). F(ab')₂ was purified by protein A affinity chromatography and after dialysis in 0.1 mol/L phosphate/0.15 mol/L NaCl (0.1 mol/L phosphate-buffered saline [PBS]), pH 7.4, was stored at 4°C.

Cross-Linking of F(ab')₂ of Z₂D₃ to F(ab')₂ of Anti-DTPA 6C31H3

An aliquot of Z₂D₃ F(ab')₂ (1–2 mg) was reacted with 14 molar excess of *N*-succinimidyl-3-(2-pyridyldithio)propionate (SPDP), and the same amount of 6C31H3 F(ab')₂ was modified with 300–1,000 times molar excess of iminothiolane (8,9). The immunoreactivities of SPDP-modified or thiolated antibodies were assessed by enzyme-linked immunosorbent assays (ELISAs) (9). Modified F(ab')₂ preparations without loss of immunoreactivity were reacted at equimolar concentration (1.75 mg) for 1 h at room temperature and then overnight at 4°C (9). The reaction mixture was then subjected to Ultrogel AcA-22 size-exclusion column (2.5 × 100 cm) chromatography (Fig. 1A). The samples were eluted from the column with 0.1 mol/L PBS. Dimeric bispecific F(ab')₂ antibodies were eluted in the first peak and the monomeric F(ab')₂ fragments were eluted in the second peak. Antibodies in these 2 peaks were subjected to sodium dodecyl sulfate–polyacrylamide gel electrophoresis (SDS–PAGE) (X Cell Sure lock Mini-Cell, Nu PAGE 6% precast gels; Invitrogen Inc.) under nonreducing condition and compared with the molecular weight standards (Fig. 1B). Nonspecific-human IgG F(ab')₂ was also cross-linked to 6C31H3 F(ab')₂ and used as nonspecific bispecific (NSB) controls.

The dimeric bispecific antibody preparations were stored at 4°C (care was taken to prevent freezing of the bispecific antibody).

Assessment of Bispecific Antibody Immunoreactivity with Surrogate Antigen (7-Dehydrocholesterol [DHC] and Benzyltrimethylhexadecylammonium Chloride [BDMHDAC])

The surrogate antigen for Z₂D₃ was prepared with minimal modification as described in U.S. patents (10,11). Briefly, to prepare antigen-coated polystyrene beads, beads with an average diameter of 3 μm (Sigma Chemical Co.) were washed and resuspended in absolute ethanol. The resulting suspension was separated into aliquots, each containing 4 μg of beads. To each aliquot, 500 μg of DHC (250 μL of a 2 mg/mL solution in ethanol) and 31 μg of BDMHDAC (31 μL of a 1 mg/mL solution in ethanol) were added. After thoroughly mixing, the solvent was allowed to evaporate at room temperature. The coated beads were stored at 4°C until they were used. The control beads were made by drying the ethanol and resuspending the beads in 0.1 mol/L PBS.

Alternatively, surrogate antigen-coated 96-well microtiter plates were also used for the assessment of the immunoreactivity of various Z₂D₃ antibody preparations as described in U.S. patent 5 811 248 (10). Briefly, aliquots of 500 μg DHC (250 μL ethanol) and 31 μg BDMHDAC (31 μL in ethanol) were mixed and added to each of the 96 wells of the microtiter plates (Beckton Dickinson & Co.). The ethanol was allowed to evaporate, and the wells were washed with PBS/Tween (0.05% Tween) (PBS-T) and then blocked with 1% horse serum, followed by additional washing. To each well, serial dilutions of bispecific or unmodified Z₂D₃

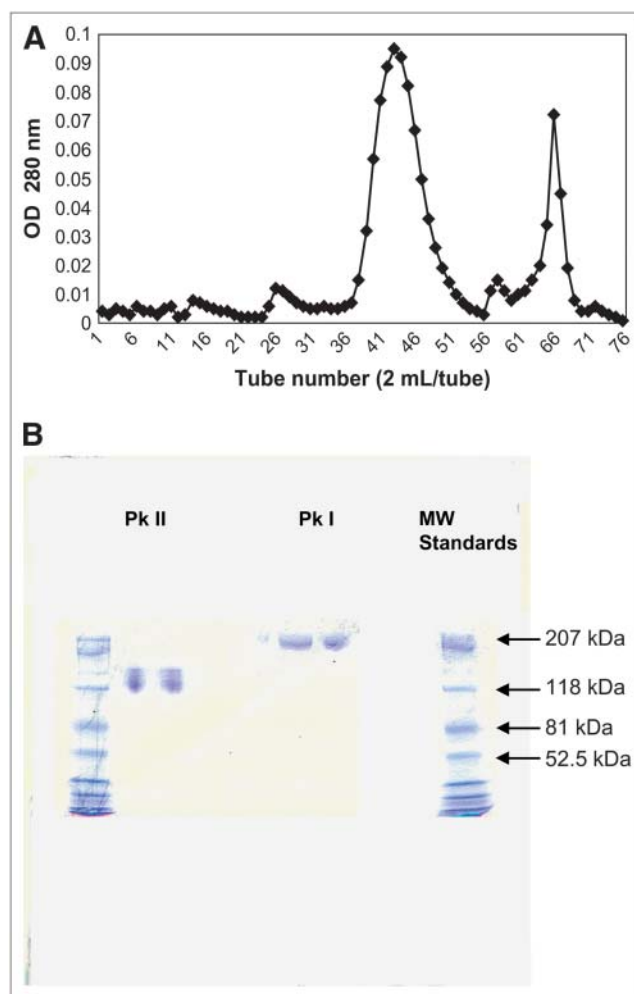


FIGURE 1. (A) Optical density (OD) 280-nm elution profile of Ultrogel-AcA-22 column chromatography for separation of bispecific antibody (peak I [Pk I] = tubes 40–50) from noncross-linked F(ab')₂ (peak II [Pk II] = tubes 64–68). (B) Nonreducing SDS–PAGE (6%) of proteins from peaks I and II from Ultrogel AcA-22 column chromatography. MW = molecular weight.

were added (10–0.0001 μg/mL) and incubated overnight at 4°C. After washing, goat antihuman IgG-conjugated horseradish peroxidase (HRP) (1:1,000 dilution) was added and incubated at 37°C for 1 h. The excess secondary antibody was washed as above, and 100 μL of *o*-phenyldiamine (OPD) (1 mg/mL OPD in 0.1 mol/L citrate, 0.2 mol/L disodium phosphate, pH 6.0) containing 30 μg/mL H₂O₂ were added to each well. After 15–30 min of incubation at room temperature in the dark, 25 μL of 2.5 mol/L H₂SO₄ were added and the optical density at 490 nm was read in an ELISA reader (EL307C; Biotech Instruments).

To determine the *in vitro* signal enhancement, serial dilutions of bispecific antibody or unmodified Z₂D₃ F(ab')₂ were added to the surrogate antigen-coated microtiter wells, prepared as described. After incubation, the unmodified Z₂D₃ binding was assessed with a secondary antibody modified with HRP as described. To test the activity of the bispecific antibody for signal enhancement, DTPA-linked PL_{46 kDa} modified with 5.5 or 9 HRP modified DTPA-PL_{46 kDa} was used (9). Incubation with the chromogen, stoppage of the reaction with H₂SO₄, and determination of the optical density were as described.

Anti-DTPA Antibody Immunoassay

Microtiter plates (96 well) were coated with 100 μL of DTPA/bovine serum albumin (BSA) (1 $\mu\text{g}/\text{mL}$) as described. The DTPA/BSA-coated wells were used to assess anti-DTPA activity by the standard ELISA protocol.

Preparation of $^{99\text{m}}\text{Tc}$ -Labeled DTPA-Suc-PL_{14.6 kDa}

An aliquot of 50 mg of polylysine (PL) (14.6 kDa; Sigma Chemical Co.) was dissolved in 5 mL of 0.1 mol/L NaHCO_3 , pH 8.7. Ten times molar excess (relative to lysine residues) of bicyclic anhydride of DTPA (Sigma Chemical Co.) in 1 mL of dimethyl sulfoxide (DMSO) was added slowly to the above solution while stirring vigorously. The number of lysyl residues modified was assessed by the trinitrobenzylsulfonic acid (TNBS) assay relative to the standard unmodified PL solution (9,12). The reaction mixture was dialyzed against excess (4 L) 0.1 mol/L carbonate, pH 9.6, at 4°C overnight. Then the DTPA-PL solution was succinylated with 100 times molar excess of succinic anhydride to modify any residual lysyl residues. The DTPA-Suc-PL_{14.6 kDa} was dialyzed in 0.1 mol/L Na_2CO_3 , pH 9.6, and stored at 4°C until used.

An approximately 50- μg aliquot of DTPA-PL_{14.6 kDa} in 0.1 mol/L Na_2CO_3 was reacted with 1,125 MBq of $^{99\text{m}}\text{Tc} - \text{O}_4^-$ in 50 μg of SnCl_2 in 100 μL of 0.1N HCl that has been flushed with N_2 for 15 min. After 30 min of incubation, the $^{99\text{m}}\text{Tc}$ -DTPA-Suc-PL_{14.6 kDa} was separated from free $^{99\text{m}}\text{Tc}$ by Sephadex-G25 (10 mL) column chromatography.

Preparation of Rhodamine-Labeled DTPA-Suc-PL_{14.6 kDa}

Rhodamine-labeled DTPA-PL was prepared by reacting 50 mg of PL_{14.6 kDa} with 3 times molar excess of DTPA anhydride (Sigma Chemical Co.) (9). The DTPA modification was assessed by the TNBS assay as before (12); then 2 mg/mL of DTPA-linked PL were reacted with 24 times molar excess of rhodamine isothiocyanate (Pierce Chemical Co.) in *N,N*-dimethylformamide (DMF). The preparation was succinylated with 100 times molar excess of succinic anhydride. The sample was dialyzed against 0.1 mol/L PBS, pH 7.4, and stored in the dark at 4°C.

In Vitro Demonstration of Specificity of Bispecific Z_2D_3 -6C31H3 with Rhodamine-Labeled DTPA-PL_{14.6 kDa}

One percent agarose gels in PBS were prepared on microscope slides. Sample wells (~2-mm diameter) were made in the gels approximately 5 mm apart. One well was filled with 75 μL of surrogate antigen-coated (DHC/BDMHDAC) beads, and the other was filled with bispecific antibody at a concentration of 1–10 $\mu\text{g}/\text{mL}$. The antibody was allowed to diffuse out of the wells overnight at 4°C. Controls consisted of unmodified beads in the first well with the same amount of bispecific antibody in the second well or surrogate antigen-coated beads in the first well and NSB control in the second well. The excess antibody or the NSB control was washed from the gels. Then the antibody or NSB control wells were filled with 50 $\mu\text{g}/\text{mL}$ of rhodamine-conjugated succinylated DTPA-PL_{14.6 kDa}. The polymers were allowed to diffuse through the gel overnight at 4°C, followed by extensive washing as described. The microscope slides were then viewed with an epifluorescent microscope (Zeiss). Fluorescent and light photomicrographs were then digitally recorded.

In Vivo Imaging Experimental Protocol

C57BL/6 mice, 8–12 wk of age with ApoE^{-/-}, were purchased from The Jackson Laboratory. Eleven ApoE^{-/-} female mice were

used to induce accelerated femoral artery atherosclerotic lesions (13) as approved by the Institutional Animal Care and Use Committee of Northeastern University. Mice were fed Western diet (21%, w/w, fat [polyunsaturated/saturated ratio = 0.07]) and 0.15%, w/w, cholesterol (Harlan Teklad) for 2 wk. Each mouse was then anesthetized with injections of intraperitoneal ketamine (90 mg/kg) and xylazine (10 mg/kg). The ventral sides of the hind legs were shaved and swabbed with butadiene and alcohol. An incision was made in the left femoral artery region. Under a surgical microscope, the femoral artery was isolated by placing 2-0 silk sutures 0.5 cm apart, isolating a segment of the femoral artery. A small incision was made with microscissors, and then a 0.25-mm-diameter angioplasty guide wire (Advanced Cardiovascular Systems) was inserted into the femoral artery segment. The guide wire was advanced and pulled back 3 times as described by Roque et al. (13) to induce endothelial injury that resulted in intimal SMC proliferative lesions. The guide wire was withdrawn and bleeding was stopped by applying pressure at the incision site for 5–10 min. The femoral incision was closed with a 3-0 silk suture using interrupted surgical knots. Antibiotic ointment (bacitracin; Denison Pharmaceuticals Inc.) was applied to the site. Similarly, the right femoral artery region underwent femoral incision and closure without endothelial injury. This right femoral artery region was used as the sham-operated control site. After surgery, all mice were returned to the cages and vital signs were monitored until the animals recovered from anesthesia. The wounds and vital signs were monitored daily until the surgical wounds were healed. ApoE^{-/-} mice with femoral endothelial denudation were kept on Western diet for an additional 2 wk. Seven mice were then injected with 30–50 μg bispecific antibody and 4 remaining mice were injected with 50 μg NSB control. The next day (~15 h later), approximately 15 MBq of $^{99\text{m}}\text{Tc}$ -DTPA-Suc-PL_{14.6 kDa} (2 μg) were injected intravenously. Anteroposterior images of the lower torso of mice were acquired using a 3-mm pinhole collimator-equipped γ -camera (Picker SX300) attached to an Apple computer with a Gamma 600 acquisition program. Ten-minute acquisition serial images at injection or between 30 min and 1 h, 1 and 2 h, and 2 and 3 h after injection of the radiotracer were obtained for each mouse. The photo peak was set at 140 keV with a 15% window. After the last imaging session, mice were euthanized by intraperitoneal injection of pentobarbital (100 mg/kg). Right and left femoral arteries were excised and rinsed in saline. Other organs (blood, heart, lungs, liver, kidneys, spleen, stomach, small and large intestine) were obtained directly for biodistribution.

Assessment of Lesion Size by Computer Planimetry

Because femoral arteries in mice are <1.0 mm in diameter, it was not practical to dissect out nonvessel adventitial tissue and other tissues from the femoral artery segment that was harvested with any efficiency. Furthermore, it was not possible to harvest atherosclerotic lesions exclusively at the time of sacrifice. Therefore, the vessel segments with the surrounding adventitia were excised, weighed, and counted in a γ -scintillation counter. To enable assessment of the atherosclerotic lesion activity without the normal adherent tissue activities, a method to estimate the percentage lesion of the whole tissue sample was developed. Ten-micron-thick frozen cross-sections of the midregion of the excised vessels and accompanying adventitia were subjected to immunoperoxidase staining using Z_2D_3 . The frozen sections were incubated with Z_2D_3 overnight, followed by washing. These sections were counterstained with rabbit antihuman IgG antibody conjugated

with HRP. After further washing, 3,3'-diaminobenzidine (DAB) substrate solution was added and incubated at room temperature for 5–10 min. The stained slides were washed extensively. The immunoperoxidase-stained slides were counterstained with methyl green, followed by washing as described. Sections were dehydrated in succession in ethanol: 70%, 75%, 95%, and 100% for 2 min each. Slides were mounted with Permount (Fisher Scientific), coverslips were applied, and then slides were viewed under light microscopy.

The immunohistochemical micrographs were photographed digitally and the digital micrographs were used to planimeter the regions of antigen-positive staining as the number of pixels and compared with the total area of the whole tissue cross-section. The percentage of the area of antigen-positive staining was determined relative to the whole tissue cross-section from 4 different left femoral arteries with lesions chosen randomly. The mean percentage of the lesion was then used to estimate the mass of the lesion in each atherosclerotic femoral artery segment.

To obtain specific lesion activity, counts per minute per gram (cpm/g) of the sham vessel (i.e., without lesion) were subtracted from the cpm/g of the lesion vessel. The nonspecific activity-corrected left femoral artery tissue activity was then divided by 0.114 (lesion = 11.4% of the whole vessel segment). Similar corrections were also made for the left femoral arteries from ApoE^{-/-} mice with atherosclerotic lesions injected with NSB control. The following formula was used:

$$\text{Corrected lesion activity} = \frac{(\text{cpm/g of lesion vessel} - \text{cpm/g of sham vessel})}{(0.114)}$$

Statistical Analysis

Data are expressed as mean \pm SD. ANOVA (single factor) was used to determine statistical significance using the statistical package of Microsoft Excell XP. A *P* value of ≤ 0.05 was considered significant.

RESULTS

The elution profile of an Ultrogel AcA-22 column chromatography is shown in Figure 1A. The first peak (tubes 40–50) in the void volume consisted of dimeric bispecific antibody F(ab')₂ complexes and the second peak (tubes 64–68) consisted of noncross-linked monomeric F(ab')₂ fragments of Z₂D₃ or 6C31H3. The molecular sizes of the dimeric bispecific F(ab')₂ relative to the second monomeric peak are shown in the 6% nonreducing SDS-PAGE (Fig. 1B). Relative to the molecular weight standards, the bispecific antibody peak consisted of dimeric F(ab')₂ (molecular weight, \sim 210 kDa), whereas the second peak consisted of an \sim 110-kDa protein band consistent with the size of monomeric F(ab')₂.

ELISA was used to determine the immunoreactivity of the dimeric bispecific (Z₂D₃-6C31H3 F(ab')₂) antibody. The surrogate antigen (Fig. 2A) or DTPA-linked BSA-coated microtiter plates were used (Fig. 2B). Binding of the bispecific antibody was compared with that of Z₂D₃ F(ab')₂ or anti-DTPA 6C31H3 F(ab')₂ using HRP-conjugated secondary antihuman or antimouse IgG antibodies, respectively. There was no difference in the binding of the bispecific

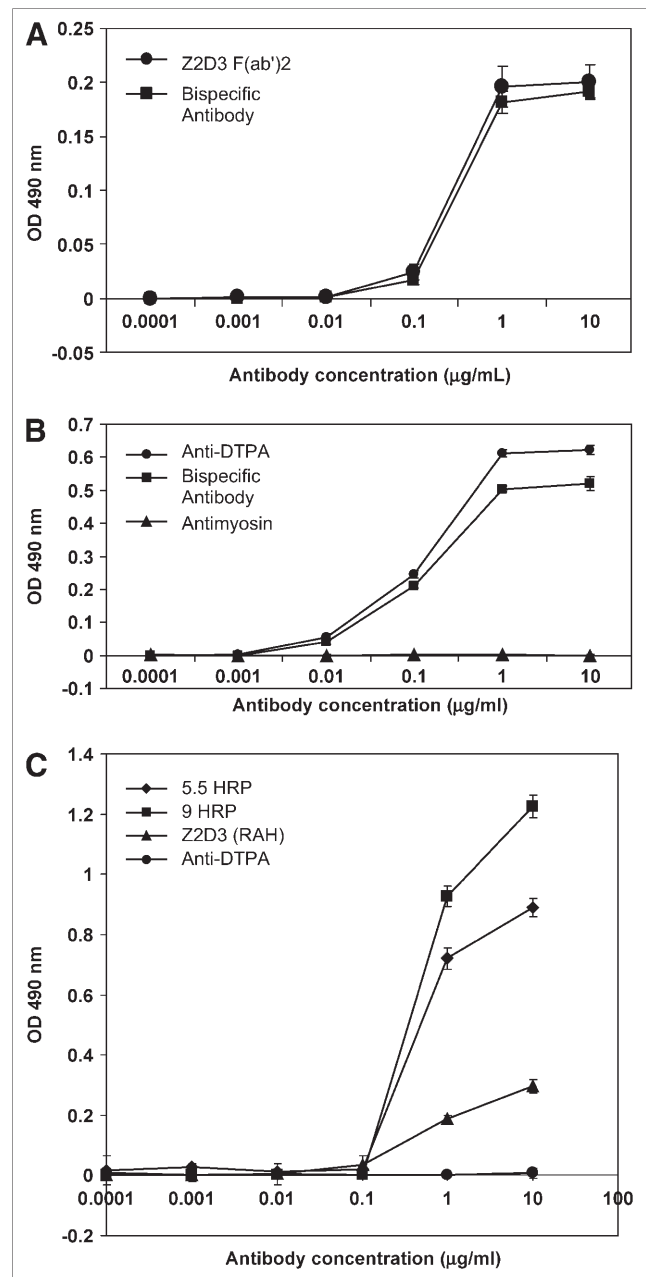


FIGURE 2. (A) Immunoreactivity of bispecific antibody and Z₂D₃ F(ab')₂ binding to surrogate antigen-coated microtiter wells by ELISA. (B) Immunoreactivity of bispecific antibody and anti-DTPA F(ab')₂ binding to DTPA-BSA antigen-coated microtiter wells by ELISA. (C) Demonstration of signal enhancement with bispecific antibody and DTPA-HRP-Suc-PL₄₆ kDa with 5.5 and 9 HRP per polymer relative to Z₂D₃ F(ab')₂ and secondary HRP-conjugated rabbit antihuman IgG antibody (RAH). Negative control is anti-DTPA F(ab')₂. OD = optical density.

antibody relative to unmodified Z₂D₃ or 6C31H3 F(ab')₂, indicating that there was no loss of immunoreactivity after formation of the bispecific antibody complexes via the disulfide linkage.

In vitro enhancement of signal with bispecific antibody was demonstrated in an ELISA with surrogate antigen-coated

microtiter plates. Antibody binding signal was assessed with DTPA–Suc–PL_{46 kDa} modified with 5.5 and 9 HRP per polymer (9) and compared with that obtained with rabbit antihuman HRP-conjugated secondary antibody (Fig. 2C). At an antibody concentration of 10 µg/mL, 4.5 and 3 times signal enhancement was obtained with 9 HRP- and 5.5 HRP-modified polymers relative to that of HRP-conjugated rabbit antihuman IgG secondary antibody. Despite the enhanced signal intensities, the background was the same for all antibody preparations.

Immunohistochemical Signal Enhancement

Frozen sections of rabbit aortas with experimental atherosclerotic lesions (6) were used to demonstrate signal enhancement by immunoperoxidase staining (Fig. 3A). The intensity of staining with 150 µg/mL of Z₂D₃ F(ab')₂ (Fig. 3A, panel e) was the same as the staining obtained between 5 and 10 µg/mL of bispecific antibody–5.5 HRP polymer (Fig. 3A, panels b and c). This resulted in 15–30 times enhancement in staining signal intensity.

In Vitro Demonstration of Specificity of Bispecific Antibody–Rhodamine-Labeled DTPA–PL for Surrogate Antigen-Coated Beads

Figure 3B shows the fluorescent and the corresponding light micrographs of surrogate antigen-coated beads (panels a and b), control nonantigen-coated beads (panels c and d) treated with bispecific antibody, and surrogate antigen-coated beads (panels e and f) treated with NSB control. Even though the same bispecific antibody was used at the same concentration, only beads with surrogate antigen coating localized the bispecific antibody that subsequently captured and retained the rhodamine-labeled DTPA–Suc–PL_{14.6 kDa} (Fig. 3B, panel a).

Radiolabeling of DTPA–Suc–PL_{14.6 kDa}

Assuming an 80% recovery of the DTPA–Suc–PL_{14.6 kDa} after Sephadex-G25 column chromatography and because only the peak tube was used for in vivo studies, 40 µg of the polymer were assumed to be recovered and only 20 µg were assumed to be in the peak tube labeled with ~150 MBq ^{99m}Tc. Each mouse was injected intravenously via the

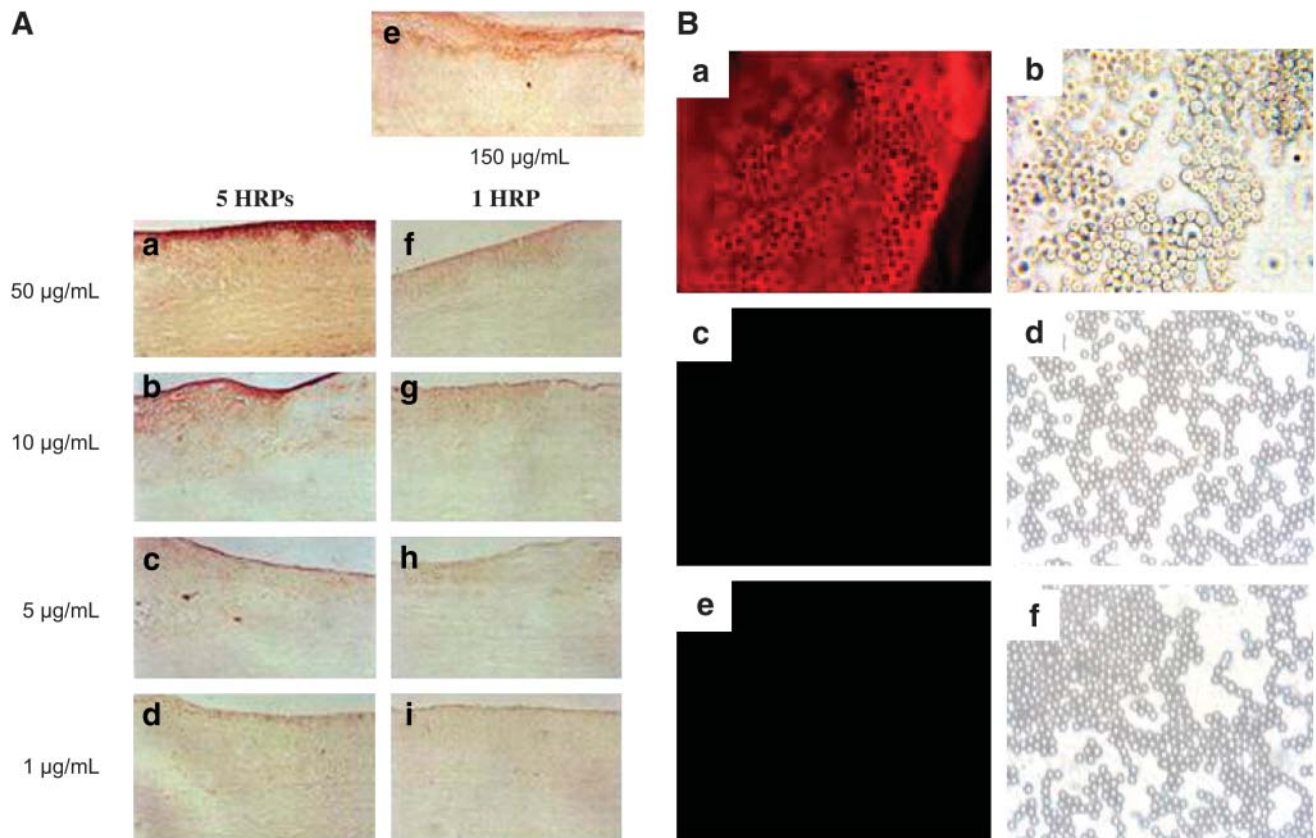


FIGURE 3. (A) Ten-micron-thick frozen sections of rabbit atherosclerotic aorta stained with 50 µg/mL (panel a), 10 µg/mL (panel b), 5 µg/mL (panel c), and 1 µg/mL (panel d) of bispecific antibody counterstained with 5.5 HRP polymer, 150 µg/mL Z₂D₃ F(ab')₂ (panel e), or 50 µg/mL (panel f), 10 µg/mL (panel g), 5 µg/mL (panel h), and 1 µg/mL of Z₂D₃ F(ab')₂ (panel i) counterstained with HRP-conjugated secondary antibody. (B) Fluorescent (panels a, c, and e) micrographs show presence or absence of rhodamine fluorescence of surrogate antigen-coated beads with bispecific antibody (panel a), empty beads with bispecific antibody (panel c), or surrogate antigen-coated beads with NSB control (panel e) targeted with rhodamine-labeled DTPA–Suc–PL_{14.6 kDa}. Corresponding light micrographs are shown in panels b, d, and f, respectively.

tail vein with ~ 15 MBq of ^{99m}Tc -DTPA-Suc-PL_{14.6} kDa (~ 2 μg ; 37 MBq is equivalent to 0.38 nmol of ^{99m}Tc).

In Vivo Imaging of Atherosclerotic Lesions in ApoE^{-/-} Mice

Figure 4A shows that there was no lesion (red arrow) or sham vessel (yellow arrow) activity in the ApoE^{-/-} mouse injected with NSB control followed by ^{99m}Tc -DTPA-Suc-PL_{14.6} kDa administration. Whereas, in the ApoE^{-/-} mouse injected with bispecific antibody followed by intravenous injection of ^{99m}Tc -DTPA-Suc-PL_{14.6} kDa, the 30-min image shows a slight increase in radioactivity in the region of the atherosclerotic lesion (Fig. 4B, left red arrow, bottom), which by 3 h became unequivocally delineated (right red arrow, bottom). There is no radiotracer accumulation in the contralateral sham-operated right leg region (yellow arrows). Furthermore, the only other organs showing radiotracer activities were the kidneys and the bladder. In the 3-h postinjection image, the lesion activity was greater than that seen in the kidneys. The 2-h postinjection ^{99m}Tc -DTPA-succinyl-PL_{14.6} kDa image in another ApoE^{-/-} mouse with an atherosclerotic lesion is shown in Figure 4C. Although there is more kidney activity, the atherosclerotic lesion is also delineated unequivocally (red arrow) and there was no activity in the contralateral sham-operated right femoral artery region (yellow arrow).

The mean pixel density \pm SD of the lesions (20.6 ± 12.21) was significantly greater than that of the contralateral sham-operated right leg regions (1.71 ± 0.76) in bispecific antibody-injected ApoE^{-/-} mice ($n = 7$) 2–3 h after ^{99m}Tc -DTPA-Suc-PL_{14.6} kDa administration ($P < 0.001$). In the NSB control injected mice, only 2 of a total of 4 mice underwent γ -imaging. The lesion activity in these mice (range, 3–4 pixels) did not differ from that of the sham-operated sites (range, 2–3). These were significantly lower than the pixel density of the lesions in bispecific antibody-injected mice ($P < 0.01$). The ratio of lesion to sham pixel density was calculated to be 12:1.

Localization of the radiotracer in the femoral arteries determined as percentage injected dose per gram (%ID/g) of total tissue mass containing the lesions is shown in Figure 5A. There was no significant difference between the mean activity in the femoral arteries with lesions (0.668 ± 0.167) and that of the sham-operated legs (0.561 ± 0.142) in mice injected with NSB control (solid bars, left to right, respectively; $n = 4$, $P =$ not significant). However, uptake of radiotracer in the whole femoral arteries with lesions in bispecific antibody-injected mice (left open bar, 2.003 ± 1.024) was significantly greater than that of the contralateral sham-operated right femoral artery (right open bar, 0.852 ± 0.368 ; $P < 0.02$) or the lesion activity (0.668 ± 0.167) of mice injected with NSB control ($P < 0.03$). The left to right femoral artery activity per gram of total vessel tissue also showed that the mean ratio in ApoE^{-/-} mice with bispecific antibody injection (2.40:1) was significantly greater than that of mice injected with NSB control (1.19:1) ($P < 0.007$).

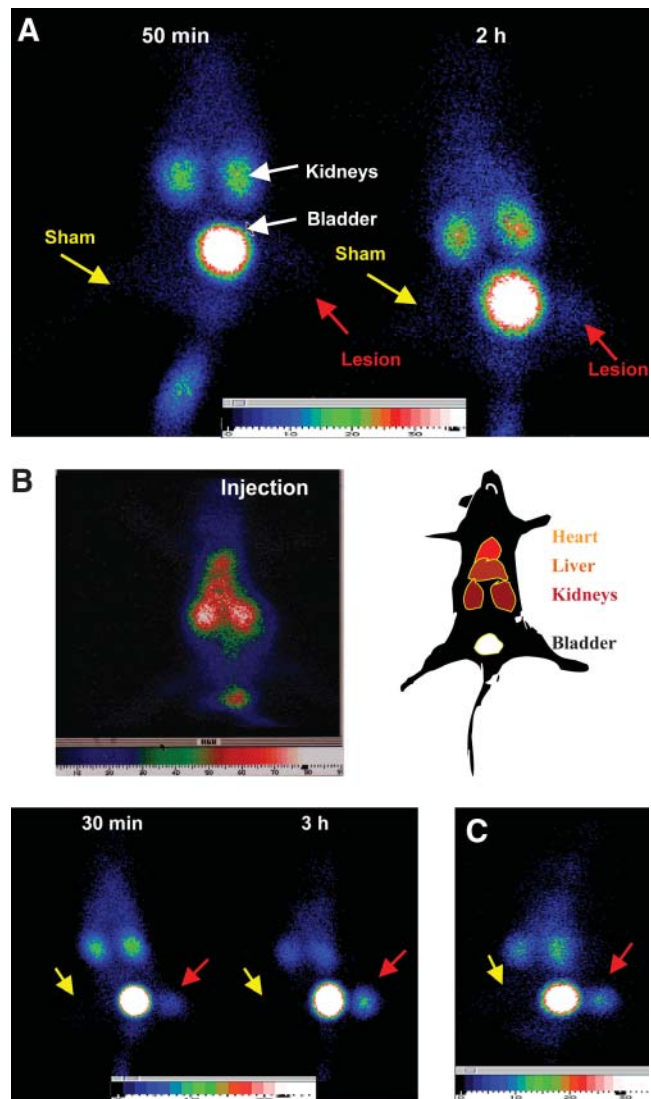


FIGURE 4. (A) Anteroposterior images of an ApoE^{-/-} mouse on Western Diet with experimental atherosclerotic lesion in left leg (red arrows) and sham-operated right leg (yellow arrows) injected with NSB control followed by ~ 15 MBq of ^{99m}Tc -DTPA-Suc-PL_{14.6} kDa. The 50-min postpolymer injection image is on left and 2-h image is on right. (B) Anteroposterior images of another ApoE^{-/-} mouse injected with bispecific antibody followed by ^{99m}Tc -DTPA-Suc-PL_{14.6} kDa injection. Top left image was obtained at injection and diagram of various organ activities is in top right. Bottom left image is 30-min image after injection of radiolabeled polymer and bottom right image is 3-h image. Red arrows denote lesion site and yellow arrows denote sham-operated site. (C) Image of another ApoE^{-/-} mouse with experimental atherosclerotic lesion 2 h after injection of ^{99m}Tc -DTPA-Suc-PL_{14.6} kDa. Red arrow = lesion; yellow arrow = sham-operated site.

The existence of neointimal lesions and the presence of antigen specific for Z₂D₃ were demonstrated by immunoperoxidase-histochemical staining. Figure 5B shows a strong dark staining in a midleft femoral artery section stained specifically with bispecific antibody (panel a), whereas there was no staining observed in the sham-operated right

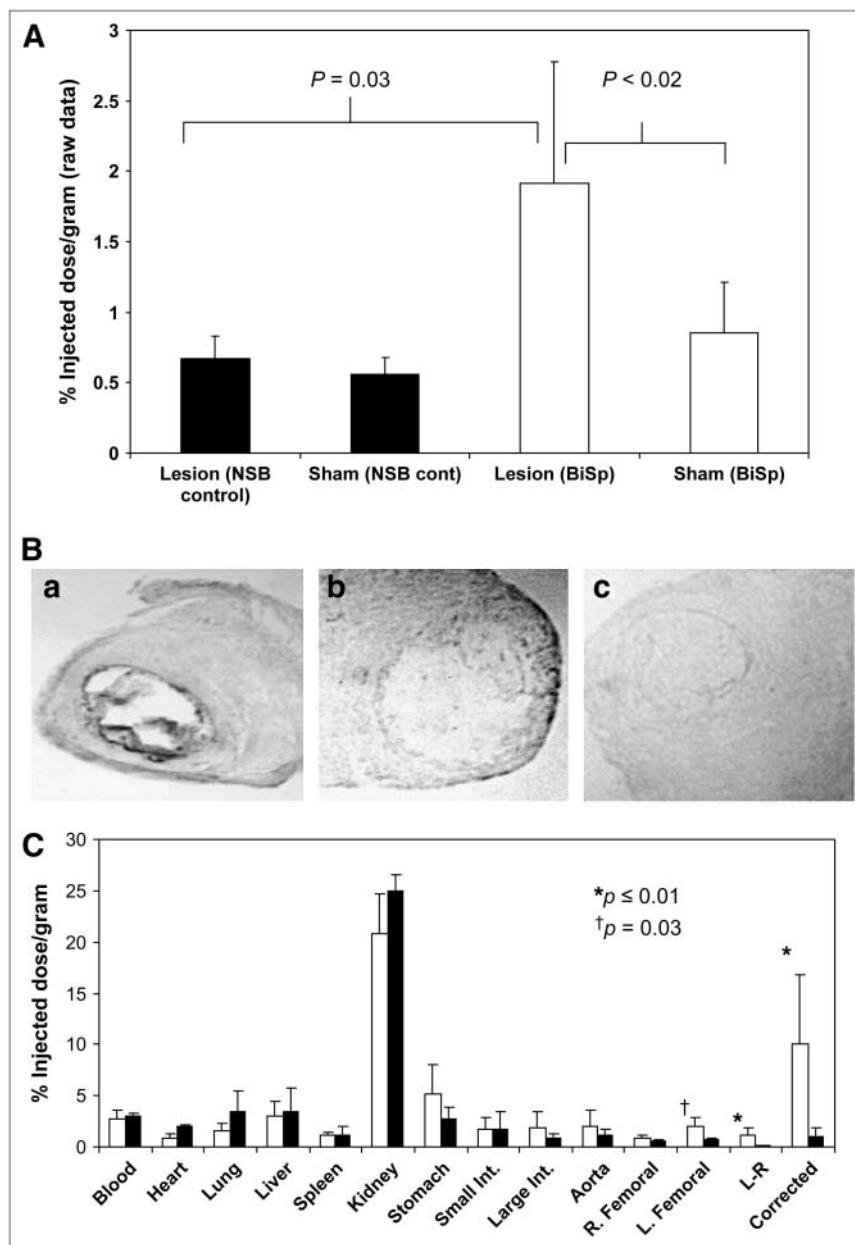


FIGURE 5. (A) Localization of radiotracer in left (lesion) and right (sham) femoral arteries determined as %ID/g of total vessel tissue samples injected with NSB control (NSB cont; solid bars) or bispecific antibody (BiSp) (open bars). (B) Immunohistochemical stained frozen sections of left femoral artery lesion with bispecific antibody (panel a), normal right femoral artery from sham-operated region with bispecific antibody (panel b), and left femoral artery (lesion) with NSB control (panel c). (C) Biodistribution of ^{99m}Tc -DTPA-Suc-PL_{14.6} kDa activity in ApoE^{-/-} mice with bispecific antibody (open bars) or NSB control (black bars). Int. = intestine; R = right; L = left.

femoral artery section (panel b). No immunohistochemical staining of the lesion vessel section was observed with the NSB control (panel c). From similar sections of 4 randomly chosen mice with lesion stained with bispecific antibody, the average areas of antigen-positive staining relative to the total area of the femoral artery sections was determined to be $11.4\% \pm 2.66\%$ by computer planimetry. This resulted in the estimation of the mean lesion size to be 2.64 ± 2.46 mg. The percentage of the mean area of antigen presence was used to correct for the presence of nonlesion tissues in the segments of the femoral arteries that were counted in the γ -scintillation counter. The corrected radioactivity of bispecific antibody ^{99m}Tc -DTPA-Suc-PL_{14.6} kDa was 10.10 ± 6.76 %ID/g of lesion and that of the NSB control in the lesion was 0.939 ± 0.877 %ID/g of lesion ($P = 0.027$) (Fig. 5C, far

right open and solid bars, respectively). The mean ratio of the corrected lesion radioactivity to sham vessel radioactivity ($0.852 + 0.368$) was calculated to be 11.85:1, which was consistent with the mean target-to-nontarget (sham) activity ratio from computer planimetry (12.05:1).

Biodistribution of ^{99m}Tc -DTPA-Suc-PL_{14.6} kDa in all ApoE^{-/-} mice determined at 2–3 h after radiotracer administration in bispecific antibody ($n = 7$, open bars) or NSB control ($n = 4$, black bars) injected mice is shown in Figure 5C. The mean radioactivity in atherosclerotic lesions containing left femoral artery of mice injected with bispecific antibody was significantly greater than the mean radioactivity of atherosclerotic lesions in mice injected with NSB control ($P = 0.03$). The difference between left and right femoral artery activities of mice injected with

bispecific antibody or NSB control was also statistically significant ($P \leq 0.01$). There was no statistical difference in other organs.

DISCUSSION

Proliferation of vascular SMCs plays a role in different stages of atherosclerotic plaque development and evolution. The American Heart Association classification of atherosclerotic lesions was recently modified and simplified by Virmani et al. on the basis of morphology (14). Mild nonatheromatous lesions include intimal thickening due to accumulation of SMCs and intimal xanthoma or fatty streak. Fatty streaks are early lesions that are flat and consist predominantly of lipid-laden macrophages and minimal numbers of SMCs. It has not been established whether these lesions are the earliest precursors of more-advanced disease and they regress or areas of smooth muscle cell presence in the "intimal cell mass" of atherosclerotic plaques are the true precursors (15). SMCs in a proteoglycan-collagen matrix with variable numbers of macrophages and lymphocytes are found in the cap of fibrous cap atheromatous lesions. Plaque vulnerability to rupture with luminal occlusion is associated with a thin cap heavily infiltrated by macrophages with rare SMCs (16). However, plaque erosion also leads to thrombotic luminal occlusion at sites of endothelial denudation overlying lesions rich in SMCs and proteoglycans (17). Plaque erosion leading to mural thrombi without occlusion results in the growth of the plaque volume (17). It is hypothesized that SMCs are involved in this lesion by becoming activated and migrating into the fibrin clot similar to fibroblasts in wound healing (18,19).

In an attempt to target the SMC proliferation component of atheromas, mice were immunized with homogenized human atherosclerotic plaques and an antibody designated as Z₂D₃ (IgM class, κ light chain) was produced. Z₂D₃ reacted specifically with intimal proliferating SMCs in human atheroma (20), experimental rabbit (6), and swine lesions (21). The parent Z₂D₃ IgM monoclonal antibody was subsequently genetically engineered to produce a murine-human chimera with a human IgG1 constant region. The F(ab')₂ of Z₂D₃ labeled with ¹¹¹In was successfully used to image rabbit atheromas at 48 h after antibody injection (6).

To improve the counts per pixel and target-to-background ratio in single-photon imaging, we have linked multiple DTPAs with PL that could chelate a large number of trivalent metallic radiolabels to Z₂D₃ (5,22). This process improved target-to-background activities by simultaneously increasing the amount of radiolabeled antibody delivered to the target and reducing the electrostatic attraction to nontarget cells with overall weak negative charge. Using ¹¹¹In-labeled PL Z₂D₃ F(ab')₂, we demonstrated that with higher antibody doses experimental lesions could be visualized earlier (5). In a phase I study, Carrio et al. showed

focal carotid uptake of ¹¹¹In-DTPA-succinylated PL-modified Z₂D₃ F(ab')₂ in patients with recent ischemic cerebral events (22).

We have now improved targeting of very small lesions while maintaining in vivo background activity to a minimum. This enabled in vivo scintigraphic visualization of small lesions (2.64 ± 2.46 mg) using a vintage clinical γ -camera equipped with a pinhole collimator. The only other organs that showed radiotracer activity were the kidneys and the bladder. Such organ activities are unavoidable, as the size of the polymers was chosen to enable elimination by renal excretion. An obstacle that we had encountered previously in the assessment of radiotracer localization was that SMC proliferation in experimental atherosclerotic lesions constitutes a very minor portion of the total vascular segment that was harvested to determine tissue activity. By staining the vascular segments containing lesions with Z₂D₃, then by planimetry the areas stained relative to the total tissue segment, we were able to normalize the activity to the estimated lesion size. It appears that, of the mean femoral mass of 22.96 ± 21.58 mg that was used for γ -scintillation counting, only $11.4\% \pm 2.66\%$ constituted antigen-positive tissue, resulting in 2.64 ± 2.46 mg of mean lesion mass. This process of normalization demonstrated that the ratio of the intensity of the lesions (20.6 ± 12.21 pixels) to sham regions (1.71 ± 0.76) of 12:1 was consistent with the ratio of the ex vivo γ -counting of 11.86:1 (10.10/0.8516). This also demonstrated that lesions as small as a few milligrams (<1 to 5 mg) can be visualized by in vivo imaging as long as there is sufficient radioactivity at the target sites and the background activity remains low, even though the resolution of the γ -camera used was not as high as that of the new rodent mini-SPECT γ -cameras. Even with the best Bioscan NanoSPECT γ -cameras, the resolution is only 0.6 mm. However, by delivering targeting radiopharmaceutical with high specific radioactivity, the ability to detect small lesions in rodents should be further enhanced.

The limitation of the current study is that the tissue sections used for immunohistochemical staining for calculation of the lesion size were assumed to be representative of the whole lesion vessel. Furthermore, only sections from 4 randomly chosen femoral arteries were used. In reality, the extent of the lesions could be more or less. Because these sections were obtained from the midregions of the lesion vessels, the extent of the lesion should be maximum. The 2 extremities of the lesion vessels would normally have less injury. Therefore, our assumption that the extent of the lesion is consistent throughout the segment of the vessel with lesion may be an overestimation of the lesion size and, therefore, an underestimation of the target activity. The only way to improve on this assumption is to undertake immunohistochemical staining of serial sections of each vessel. Nonetheless, the activity ratio of the target to sham-operated region from computer planimetry of in vivo images was similar to that obtained after correction of lesion mass

by γ -scintillation counting, indicating that both methods of lesion assessment are comparable.

Although the specific radioactivity that is used in these studies has not been optimized, the present study showed the potential of using bispecific antibodies with ^{99m}Tc -labeled negatively charged polymers for enhanced in vivo imaging. Radiolabeling at 5.4–140 MBq/ μg of polymers or 1–5.5 mol of ^{99m}Tc per mol of polymer radiospecific activity has been achieved (data not shown). In the current in vivo studies, 7.5 MBq/ μg of polymer were used. Most radiopharmaceuticals labeled with ^{99m}Tc used higher concentrations of the pharmaceuticals. In the glucuronic acid kits used for imaging acute myocardial infarction (23), 12.5 mg of glucuronic acid were labeled with 1,125 MBq ^{99m}Tc . Assuming 100% labeling efficiency, the specific activity would be 0.09 MBq/ μg of glucuronic acid. This is 2.3×10^{-4} mol ^{99m}Tc per mol of glucuronic acid. Therefore, the polymers were radiolabeled with ^{99m}Tc at a relatively high specific activity (~ 83 –1,400 times more efficient than ^{99m}Tc labeling of glucuronic acid). Furthermore, because the polymer is the molecule that is radiolabeled, the problems associated with radiolabeling of antibodies are avoided.

CONCLUSION

Use of bispecific antibody complex with radiolabeled polymer enabled high specific radioactivity targeting at femoral atherosclerotic lesions in ApoE^{-/-} mice, allowing unequivocal visualization of the lesions by γ -imaging within 2 h. Substitution of single-photon radioisotopes with other signaling molecules may allow pretargeted imaging with positron-emission radioisotopes or paramagnetic ions for enhanced MRI. Substitution with therapeutic agents on these polymers may result in more efficient therapy similar to the use of bispecific antibodies and radiotherapeutic iodine-labeled dipeptides (24).

ACKNOWLEDGMENT

This study was partially supported by the NIH grant HL060785.

REFERENCES

1. Brennan M, Davison PF, Paulus H. Preparation of bispecific antibodies by chemical recombination of monoclonal immunoglobulin G1 fragments. *Science*. 1985;229:81–83.
2. Le Doussal JM, Martin M, Gautherot E, Delaage M, Barbet J. In vitro and in vivo targeting of radiolabeled monovalent and divalent haptens with dual specificity monoclonal antibody conjugate: enhanced divalent hapten affinity for cell-bound antibody conjugate. *J Nucl Med*. 1989;30:1358–1366.
3. Le Doussal JM, Gruaz-Guyon A, Martin M, et al. Targeting of indium-111-labeled bivalent hapten to human melanoma by bispecific monoclonal antibody conjugates: imaging of tumors hosted in nude mice. *Cancer Res*. 1990;50:3445–3452.

4. Karacay H, McBride WJ, Griffiths GL, et al. Experimental pretargeting studies of cancer with a humanized anti-CEA X murine anti-(In-DTPA) bispecific antibody construct and a ^{99m}Tc -/ ^{188}Re -labeled peptide. *Bioconj Chem*. 2000; 11:842–854.
5. Narula J, Petrov A, Ditlow C, et al. Maximizing radiotracer delivery to experimental atherosclerotic lesions with high-dose, negative charge-modified Z2D3 antibody for immunoscintigraphic targeting. *J Nucl Cardiol*. 1997;4: 226–233.
6. Narula J, Petrov A, Bianchi C, et al. Noninvasive localization of experimental atherosclerotic lesions with mouse/human chimeric Z2D3 F(ab')₂ specific for the proliferating smooth muscle cells for human atheroma. *Circulation*. 1995;92: 474–484.
7. Rousseaux J, Rousseaux-Prevost R, Bazin H. Optimal conditions for the preparation of proteolytic fragments from monoclonal IgG of different rat IgG subclasses. *Methods Enzymol*. 1986;121:663–669.
8. Bush DA, Winkler MA. Isoelectric focusing of cross-linked monoclonal antibody heterodimers, homodimers, and derivatized monoclonal antibodies. *J Chromatogr*. 1989;489:303–311.
9. Khaw BA, Rammohan R, Abu-Taka A. Bispecific enzyme-linked signal-enhanced immunoassay with subatto-moles sensitivity. *Assay Drug Dev Technol*. 2005;3:319–327.
10. Ditlow CC, Chen FW, Calenoff E, inventors. Charter Ventures, assignee. Atherosclerotic plaque specific antigens, antibodies thereto, and uses thereof. US patent 5 811 248, September 22, 1998.
11. Ditlow CC, Chen FW, Calenoff E, inventors. Charter Ventures, assignee. Atherosclerotic plaque specific antigens, antibodies thereto, and uses thereof. US patent 5 955 584, September 21, 1999.
12. Habeeb AFSA. Determination of free amino groups in proteins by trinitrobenzenesulfonic acid. *Anal Biochem*. 1966;14:328–336.
13. Roque M, Fallon JT, Badimon JJ, et al. Mouse model of femoral artery denudation injury associated with the rapid accumulation of adhesion molecules on the luminal surface and recruitment of neutrophils. *Arterioscler Thromb Vasc Biol*. 2000; 20:335–342.
14. Virmani R, Kolodgie FD, Burke AP, Farb A, Schwartz SM. Lessons from sudden coronary death: a comprehensive morphological classification scheme for atherosclerotic lesions. *Arterioscler Thromb Vasc Biol*. 2000;20:1262–1275.
15. Thomas WA, Reiner JM, Florentin RA, Lee KT, Lee WM. Population dynamics of arterial smooth muscle cells. V. Cell proliferation and cell death during initial 3 months in atherosclerotic lesions induced in swine by hypercholesterolemic diet and intimal trauma. *Exp Mol Pathol*. 1976;24:360–374.
16. Bjorkerud S, Bjorkerud B. Apoptosis is abundant in human atherosclerotic lesions, especially in inflammatory cells (macrophages and T cells) and may contribute to the accumulation of gruel and plaque instability. *Am J Pathol*. 1996;149:367–380.
17. Burke AP, Kolodgie FD, Farb A, et al. Healed plaque ruptures and sudden coronary death: evidence that subclinical rupture has a role in plaque progression. *Circulation*. 2001;103:934–940.
18. Yee KO, Schwartz SM. Why atherosclerotic vessels narrow: the fibrin hypothesis. *Thromb Haemost*. 1999;82:762–771.
19. Geary RL, Nikkari ST, Wagner WD, et al. Wound healing: a paradigm for lumen narrowing after arterial reconstruction. *J Vasc Surg*. 1998;27:96–106.
20. Harrison DC, Calenoff E, Chen FW, Parmley WW, Khaw BA, Ross R. Plaque-associated immune reactivity as a tool for the diagnosis and treatment of atherosclerosis. *Trans Am Clin Climatol Assoc*. 1992;103:210–217.
21. Johnson LL, Schofield LM, Weber D, Kolodgie F, Virmani R. Uptake of ^{111}In -Z2D3 on SPECT imaging in a swine model of coronary stent restenosis correlated with cell proliferation. *J Nucl Med*. 2004;45:294–299.
22. Carrio I, Pieri PL, Narula J, et al. Noninvasive localization of human atherosclerotic lesions with indium 111-labeled monoclonal Z2D3 antibody specific for proliferating smooth muscle cells. *J Nucl Cardiol*. 1998;5: 551–557.
23. Khaw BA, Nakazawa A, O'Donnell SM, Pak KY, Narula J. Avidity of ^{99m}Tc -glucarate for the necrotic myocardium: in vivo and in vitro assessment. *J Nucl Cardiol*. 1997;4:283–290.
24. Van Schaijk FG, Boekema M, Oosterwijk E, et al. Residualizing iodine markedly improved tumor targeting using bispecific antibody-based pretargeting. *J Nucl Med*. 2005;46:10161022.